RESEARCH ARTICLE

NANO · MICRO small
www.small-journal.com

Graphitized Layers Encapsulated Carbon Nanofibers as Li-Free Anode for Hybrid Li-Ion/Metal Batteries

Taiyu Lyu, Lizhe Liang, Kaige Liu, Fenqiang Luo, Qianyu Fan, Peiwan Guo, Dechao Wang,* Guozhen Wei, Lei Tao,* and Zhifeng Zheng**

Hard carbon, the Li-free anode for hybrid Li-ion/metal batteries (LIB/LMBs), has great potential for enhancing fast charging capability, energy density, and battery lifespan. However, low initial Coulombic efficiency (ICE) and Li dendrite growth are crucial factors constraining its development. In this work, graphitized layers encapsulated carbon nanofibers (G-CF) are fabricated via Joule heating within 10 s. The C_{sp2} structure in graphitized layers reduces side reactions with the electrolyte, promotes LiC compound formation, and improves Li ions/metal reversibility. The inner amorphous carbon structure boosts fast charging capability. As a result, the G-CF anode attains an 85.2% high ICE and exhibits long-term cycling stability. Under 2 C fast charging, it maintains an average Coulombic efficiency of 99.94% and a 500 mAh g^{-1} capacity after 200 cycles. Moreover, when the N/P ratio is 0.5, the G-CF||NCM811full cell has an ICE of 84.5% and provides a capacity of 530.8 mAh g^{-1} and an energy density of 365.9 Wh kg^{-1} at 1C. The G-CF||LFP full cell can also provide a capacity of 541.0 mAh g^{-1} under the same N/P ratio. A 30 mAh pouch cell can stably cycle over 100 times. This heterogeneous hard carbon design paves a revolutionary path for manufacturing high-efficiency Li-free anodes for hybrid LIB/LMBs.

1. Introduction

In the current era of rapid global economic development, renewable energy demand is witnessing a sharp increase, and the significance of energy storage technology is becoming increasingly prominent.[1–3] Traditional Li-ion batteries have played a crucial role in the past.[4] However, they struggle to meet the strong demands of the future market for fast charging capability and extremely high energy density. The Li metal anode, with its advantages of low density (0.53 g cm^{-3}), high theoretical specific capacity (≈3860 mA h g^{-1}), and extremely low reduction potential (≈3.04 V), is an ideal choice for the next generation of Li-ion batteries.[5,6] Nevertheless, the issues of low Coulombic efficiency (CE) and Li dendrite growth seriously restrict its development.[7,8]

As a Li metal substrate, carbon materials have been confirmed to facilitate the formation of carbon/Li metal composite anodes, effectively reducing Li metal consumption and inhibiting the growth of Li dendrites.[5,9,10] However, under a low N/P ratio, the full cell has difficulty achieving stable cycling hundreds of times.[11–13] Hybrid Li-ion/metal batteries (LIB/LMBs) are the new solution that uses less carbon materials as an anode for Li-ion/metal storage and have higher energy density than traditional Li-ion batteries (see Scheme S1, Supporting Information). This not only reduces costs but also avoids the strict environmental requirements for preparing carbon/Li metal composite anodes.[14,15] However, the carbon substrate has a limited ability to store Li

T. Lyu, F. Luo, Q. Fan, P. Guo, D. Wang, Z. Zheng
Fujian Provincial Industry Technologies Development Base for New Energy
Collaborative Innovation Platform for Energy Storage Technology of Advanced Electrochemical of Fuzhou-Xiamen-Quanzhou National Independent Innovation Demonstration Zone
College of Energy
Xiamen University
Xiamen 361102, P.R. China
E-mail: fqluo@stu.xmu.edu.cn; wangdechao@xmu.edu.cn; zhifeng.zheng@xmu.edu.cn

L. Liang
School of Mechanical Engineering
Guangxi University
Nanning 530004, P.R. China

The ORCID identification number(s) for the author(s) of this article can be found under https://doi.org/10.1002/smll.202412457

DOI: 10.1002/smll.202412457

K. Liu
State Key Laboratory of Physical Chemistry of Solid Surfaces
Collaborative Innovation Center of Chemistry for Energy Materials
College of Chemistry and Chemical Engineering
Xiamen University
Xiamen 361102, P.R. China

G. Wei
XTC New Energy Materials (Xiamen) LTD.
300-3, Kejingshe, Xiamen 361026, P.R. China

L. Tao
Department of Chemistry
Virginia Tech
Blacksburg, VA 24061, USA
E-mail: taolei@vt.edu

Z. Zheng
China Fujian Innovation Laboratory of Energy Materials Science and Technology
Tan Kah Kee Innovation Laboratory
Xiamen University
Xiamen 361102, P.R. China

ions, especially in the voltage range of 0–0.1 V where almost no Li-ion intercalation occurs.[16–18] This causes a large amount of Li metal to participate in the reaction and accelerates its consumption.

In recent years, electrolyte design has played a crucial role in increasing the Li-ion intercalation capacity and improving the stability of hybrid LIB/LMBs. Our team reported the anion-dominated weakly solvating electrolyte that can endow the carbon anode with ultra-high low-potential capacity and high average CE.[19] Moreover, the pre-cycled carbon anode can stably cycle more than a thousand times in a hybrid battery. However, surface defects on carbon materials can cause strong side reactions with the electrolyte and affect the initial Coulombic efficiency (ICE).[20–22] Although pre-cycling or Li replenishment strategies can improve the ICE of hard carbon anodes to a certain extent, the complex procedures hinder large-scale applications.

In this work, we fabricated graphitized layers encapsulated carbon nanofibers (G-CF) through flash Joule heating within just 10 seconds (s). Comprehensive theoretical modeling and rigorous experimental evidence highlight the crucial role of C_{sp^2} carbon configurations in graphitized outer layers in mitigating side reactions between the electrolyte and electrode. This heterogeneous structure design not only promotes the formation of LiC compound and enhances the reversibility of Li-ion/metal storage but also the amorphous carbon structure in the inner layer guarantees rapid charging capability. By utilizing regular Li-ion storage and then electroplating 300 mAh g^{-1} of Li below 0 V to form hybrid Li-ion/metal storage behavior, the G-CF anode exhibits an ICE of 85.2% and long cycling stability in ether-based electrolyte (1M LiFSI-tetrahydrofuran (LiFSI-THF)). Under 2C fast charging, the G-CF anode shows an average CE of 99.94% and a 500 mAh g^{-1} capacity after 200 cycles. When the N/P ratio is 0.5, the full cell also provides remarkable cycling performance. This exceptional performance significantly amplifies the advantages of hard carbon as a carbon/Li composite anode in Li metal batteries (LMBs) or as a Li-free anode in hybrid LIB/LMBs, highlighting the transformative potential of our G-CF design.

2. Results and Discussion

2.1. Fabrication and Characterization

Figure 1a presents the schematic diagram of the flash Joule heating experiment. It involves ultrafast heating, maintaining a stable temperature of 1200 °C for 5 s, followed by ultrafast cooling. The entire process lasts no >10 s. As shown in Figure 1b, the CF is fabricated by carbonizing the CF precursor in a traditional tube furnace at 1200 °C for 2 h.[23] Subsequently, flash Joule heating at 1200 °C for 5 s is performed, and the resulting CF is labeled as G-CF (experimental section and Figure S1, Supporting Information). Scanning electron microscopy (SEM) is employed to observe the surface morphologies of CF and G-CF. Both exhibit an intertwined nanofiber network (Figure 1c,d), which is beneficial for rapid electron transfer and enhances electrolyte infiltration (Figure S2, Supporting Information).[19,24] It also effectively mitigates the volume expansion of Li metal during the charge–discharge process of hybrid LIB/LMBs. High-resolution transmission electron microscopy (HRTEM) is utilized to analyze the microstructure of CF and G-CF. The CF has a typical amorphous carbon structure (Figures 1c1–c3 and S3, Supporting Information). However, after flash Joule heating, the G-CF shows an obvious heterogeneous structure, with an amorphous core structure and ≈30 nm thick graphitized out layers (Figures 1d1–d3 and S3, Supporting Information). It should be noted that the thickness of the graphitized layers is influenced by flash joule heating time or temperature. For example, increasing the heating duration at 1200 °C leads to thicker graphitized layers (Figure S4, Supporting Information).

The XRD spectra show broad peaks around 22° and 42° (Figure 1e), indicating that CF and G-CF are amorphous carbon.[25] The Raman spectra have D and G bands at 1340 and 1587 cm^{-1}, respectively (Figure 1f). The D band, originating from asymmetric vibrations in six-membered carbon rings, shows that there are a large number of defects in carbon materials, while the G band indicates the presence of an ordered graphite structure.[26,27] Notably, the I_G/I_D ratio of G-CF is 1.0, exceeding that of CF (I_G/I_D = 0.9), indicating a higher degree of graphitization order. The G-CF with a higher-ordered graphitized structure exhibits a higher electrical conductivity (6.76 S cm^{-1}) than CF, which is beneficial for rapid electron transfer (Figure S5, Supporting Information). XPS analyzed the surface compositions of CF and G-CF. As depicted in Figure 1g and Table S1 (Supporting Information), the surface of CF is composed of 85.9% C and 12.5% O, while G-CF displays a significantly higher C content of 96.7% and a reduced O content of 1.7%. Depth profiling XPS was applied to investigate the composition of the surface layers of nanofibers. As the etching depth reaches 50 nm (after 175s of etching), the C atomic ratio of G-CF exceeds 96%, which is significantly better than 91.7% of CF at the same depth. Furthermore, the C 1*s* shows that the surface of G-CF has a higher proportion (58.8%) of C_{sp2} and a lower proportion of C_{sp3} carbon structures compared to that of CF (Figure 1h and Table S2, Supporting Information).[28,29] The O 1*s* of G-CF exhibit a lower O atomic ratio and a lower proportion of C═O compared to that of CF (Figures 1g and S6, Supporting Information).[30] Meanwhile, the N_2 adsorption/desorption results show that the specific surface area of G-CF decreased from 14.7 to 9.9 m^2 g^{-1} compared to CF (Figure S7, Supporting Information). These results indicate that the surface defects of G-CF are significantly reduced, minimizing the side reactions during the formation of the SEI layer.[31,32] In addition, these characterization results also confirm that nanofibers encapsulated with graphitized layers are successfully prepared by flash Joule heating.

2.2. Electrochemical Performance

The electrochemical performance of CF and G-CF electrodes with distinct surface characteristics was evaluated for hybrid Li-ion/metal storage achieved through normal full discharge to 0 V and further plating of 300 mA h g^{-1} Li below 0 V. The ICE, average CE, capacity, and long-term cycling stability are crucial parameters for judging the performance of hybrid Li-ion/metal storage. In **Figure 2a**, the average ICEs of CF and G-CF electrodes were obtained by repeating five cells. The G-CF electrode exhibits an average ICE of 85.2% at 0.2 C (1C = 500 mA g^{-1}), surpassing that of the CF electrode (76.5%). Meanwhile, compared with previously reported literature (Figure 2b), the G-CF electrode also

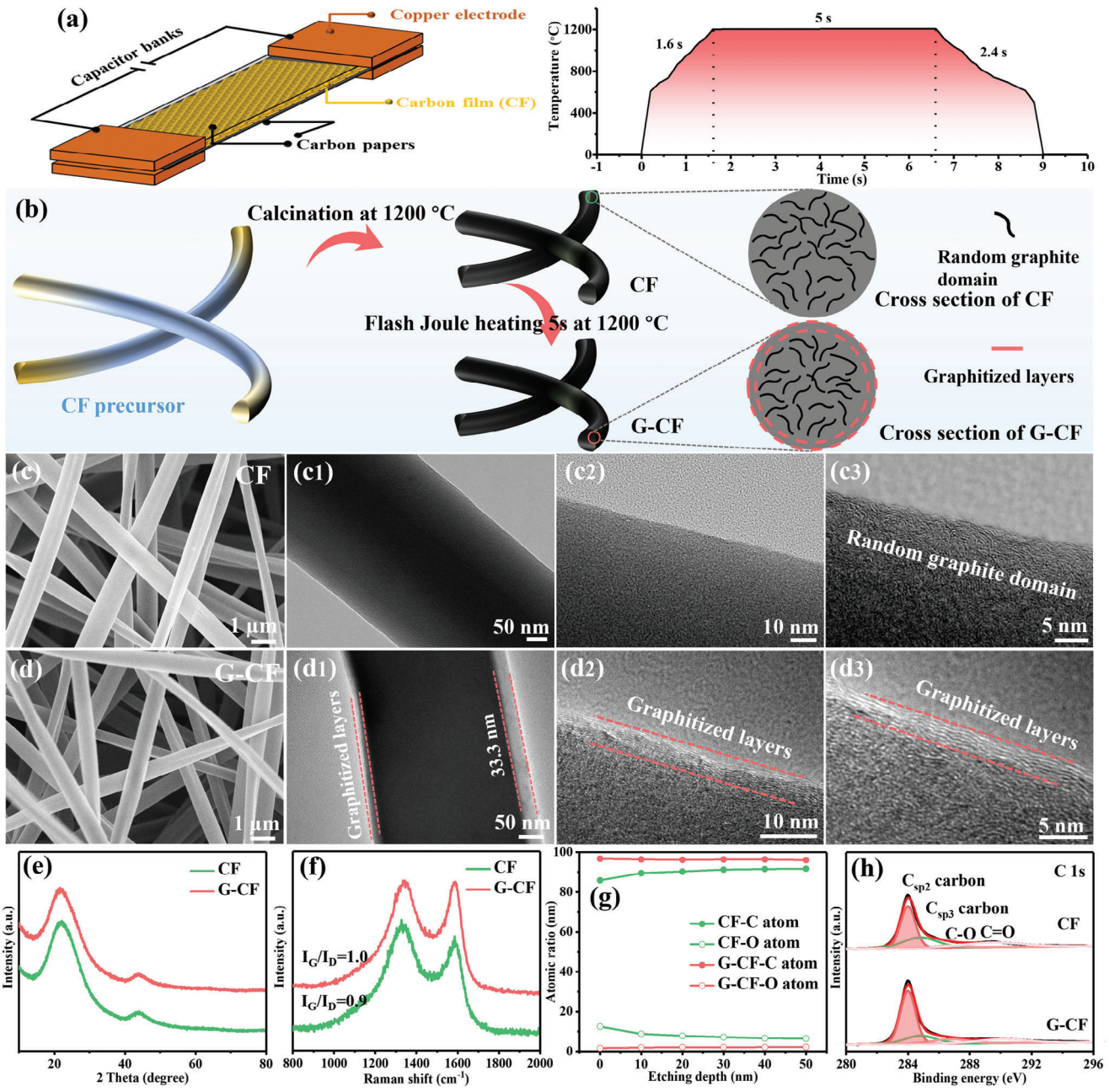

Figure 1. a) A schematic diagram of the principle of flash Joule heating and the preparation of the G-CF electrode through flash Joule heating within 10 s. b) The preparation methods and structural diagrams of CF and G-CF. SEM images of the c) CF and d) G-CF. HRTEM images of the c_1–c_3) CF and d_1–d_3) G-CF. e) The XRD spectra and f) Raman spectra of the CF and G-CF. g) The atomic ratios of C and O in CF and G-CF at different etching times. h) The high-resolution C 1s spectra on the surfaces of CF and G-CF.

shows the best ICE.[33–40] This outstanding ICE can be attributed to the graphitized layers on the nanofibers' surface, which possess a higher C_{sp2} carbon structure and a lower specific surface area, thereby mitigating detrimental side reactions between electrode and electrolyte (detailed discussion in section 2.3). The G-CF electrode also demonstrates excellent rate performance. At 0.2, 0.5, 1, and 2 C, the average CEs and capacities (within 10 cycles) are 98.87% (680.4 mA h g^{-1}), 99.37% (634.3 mA h g^{-1}), 99.57% (545.3 mA h g^{-1}), and 99.66% (486.3 mA h g^{-1}), respectively. When returning to 0.2 C, it maintains a high average CE of 99.71% and a capacity of 653.9 mA h g^{-1} (Figure 2c). In contrast, although the CF electrode exhibits comparable capacity in the rate performance test, it lags significantly behind in terms of ICE and average CE. Additionally, based on the 5th discharge curve at each current density (Figure 2d), the G-CF electrode delivers a slope capacity (0.1-2 V), a low-potential capacity platform (0-0.1 V), and a platform for plating 300 mA h g^{-1} Li (below 0 V). Importantly, the G-CF electrode exhibits an excellent low-potential

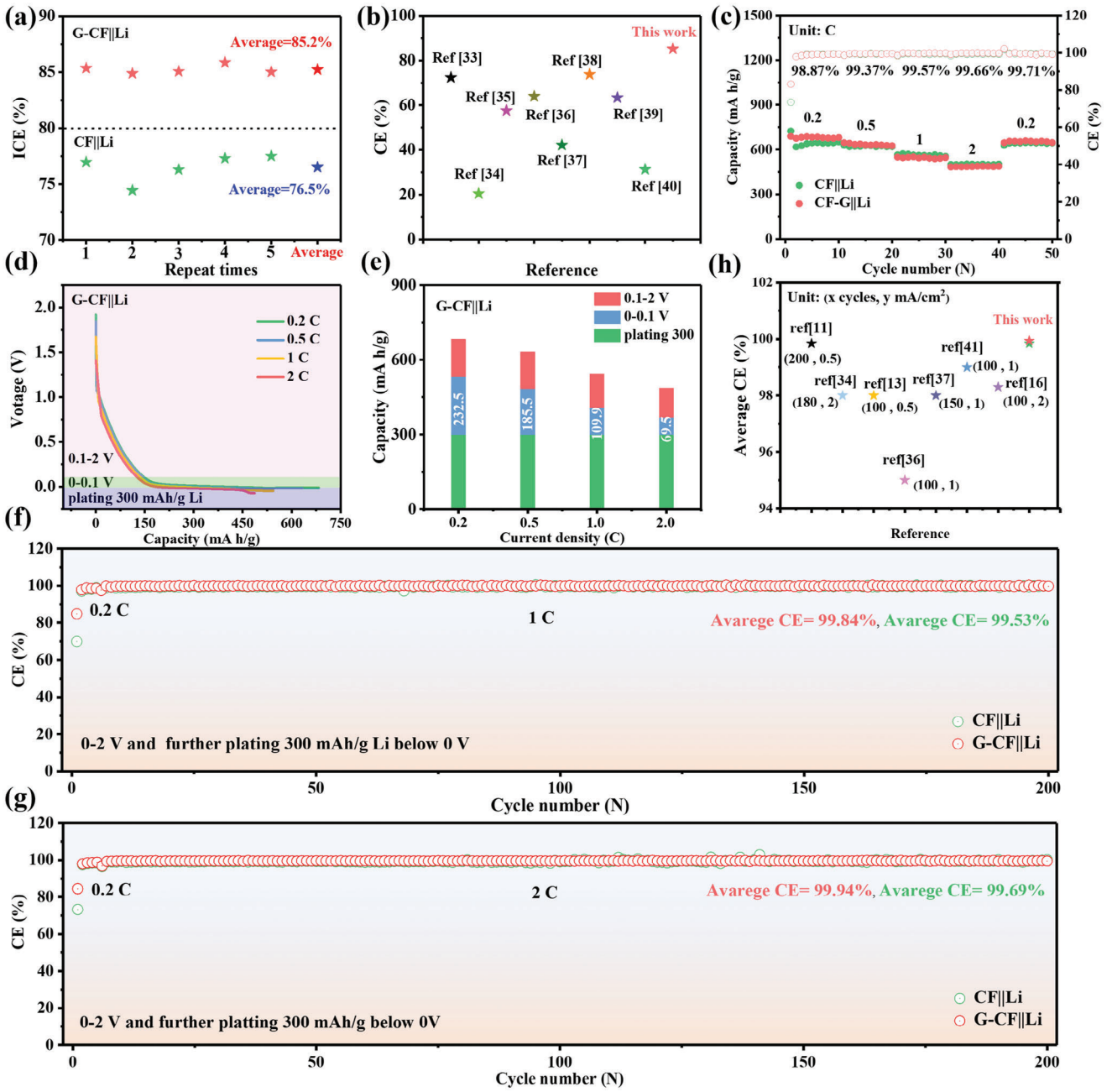

Figure 2. a) The average ICE is obtained by repeating 5 cells at 0.2 C. b) Comparison with the ICE in the reported literature. (c) Rate performance. d) The 5th discharge curves of G-CF||Li, e) the corresponding slop capacity (2–0.1 V), low-potential capacity (0.1–0 V), and plating 300 mA h g^{-1} Li (< 0 V) of G-CF||Li at different current densities. The average CE of G-CF||Li and CF||Li at (f) 1 C and (g) 2 C. h) Comparison with the average CE in the reported literature.

capacity of 232.5 mA h g^{-1} at 0.2 C (Figure 2e), which is consistent with the analysis of the cyclic voltammetry (CV) results (Figure S8, Supporting Information). Moreover, the G-CF electrode maintains a low-potential capacity at all current densities. The high low-potential capacity is due to the anion-dominated weakly solvating structure electrolyte derived from tetrahydrofuran, which realizes the co-intercalation of solvated Li^+.[19]

The long-term cycling stability test aims to evaluate the stability of hybrid Li-ion/metal storage using CF and G-CF electrodes. At 1 C, the G-CF||Li provides an average CE of 99.84% and a capacity of ≈550 mA h g^{-1} over 200 cycles (Figures 2f and S9, Supporting Information). As the current density increased to 2 C, the G-CF||Li achieves an average CE of 99.94% and maintains a capacity of over 500 mA h g^{-1} within 200 cycles (Figures 2g and S10, Supporting Information). In addition, even compared to the average CEs reported in the literature (Figure 2h), the G-CF||Li cell also shows the optimum average CE within 200 cycles.[11,13,16,34,36,37,41] On the contrary, although the CF||Li shows

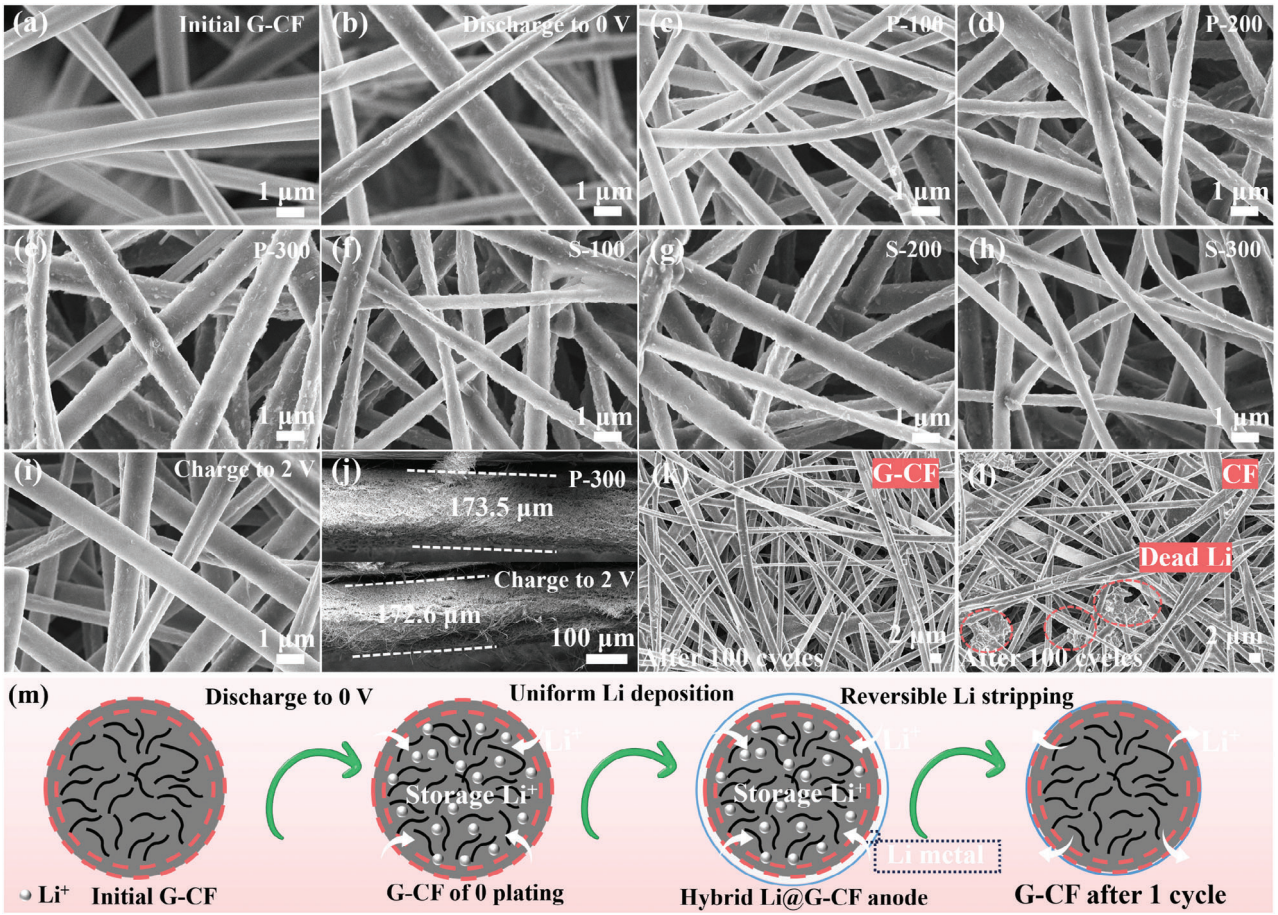

Figure 3. SEM images of the G-CF electrode of a) initial, b) full discharge to 0 V, further plating c) 100 mA h g^{-1} Li, d) 200 mA h g^{-1} Li, and e) 300 mA h g^{-1} Li below 0 V, then stripping f) 100 mA h g^{-1} Li, g) 200 mA h g^{-1} Li, h) 300 mA h g^{-1} Li, and i) full charge to 2 V again. j) Changing in the cross section during the plating 300 mA h g^{-1} Li and full charge to 2 V again. SEM images of the k) G-CF and (l) CF electrodes after 100 cycles at 2 C. m) Scheme of hybrid Li-ion/metal storage behavior of the G-CF electrode.

similar capacity in the early cycles, its average CE is lower than that of the G-CF||Li at 1 C and 2 C, eventually leading to rapid capacity deterioration (Figures 2f,g and S9,S10, Supporting Information). These results indicate that encapsulating nanofibers with graphitized layers not only improves the ICE but also maintains the stability of the G-CF electrode.

The disparity in long-term cycling stability can be further visualized by inspecting the morphological alterations that take place during or after Li plating/stripping. In **Figure 3**, SEM images unveil the morphological evolution of the G-CF electrode during the process of hybrid Li-ion/metal behavior. The initial G-CF electrode presents a network of interwoven nanofibers with a smooth surface (Figure 3a). As discharged to 0 V, the surface of the nanofibers remains smooth despite forming the SEI layer by the interaction between the nanofibers surface and electrolyte (Figure 3b). When 300 mA h g^{-1} Li was gradually plated on the G-CF electrode below 0 V, Li nucleates, grows, and envelops the surface of the nanofibers homogeneously. No chunky, aggregated, or dendritic Li was observed (Figure 3c–e). During the stripping and charging process to 2.0 V, the Li plated on the nanofibers can be reversibly removed, restoring the smooth surface of the nanofibers once again (Figure 3f–i). In addition, during the hybrid Li ions/metal storage, the thickness of G-CF electrode scarcely changes, confirming that the self-supporting G-CF electrode can effectively restrain volume expansion (Figure 3j). Even after 100 cycles at 2 C, the nanofibers of G-CF electrode retain their cleanliness, free from any traces of dead Li (Figure 3k). Conversely, the CF electrode presents block-shaped dead Li, indicating the CF electrode undergoes uneven Li plating with low reversibility (Figure 3l). A simplified visualization of reversible hybrid Li-ion/metal storage is shown in Figure 3m. The graphitized layers of G-CF can effectively reduce the side reactions of the electrolyte, enabling Li ions to be sequestered within the nanofibers' robust hard carbon framework. As Li deposition begins, Li gradually uniformly deposits and grows on the surface of the nanofibers. Subsequently, the deposited Li can be reversibly stripped off.

2.3. Storage Mechanism, SEI Properties, and Simulation

Ex situ XRD was conducted to elucidate the storage mechanism of G-CF and CF electrodes in hybrid LIB/LMBs. As shown in **Figure 4a**, during the discharge proceeds, Li ions are stored in the

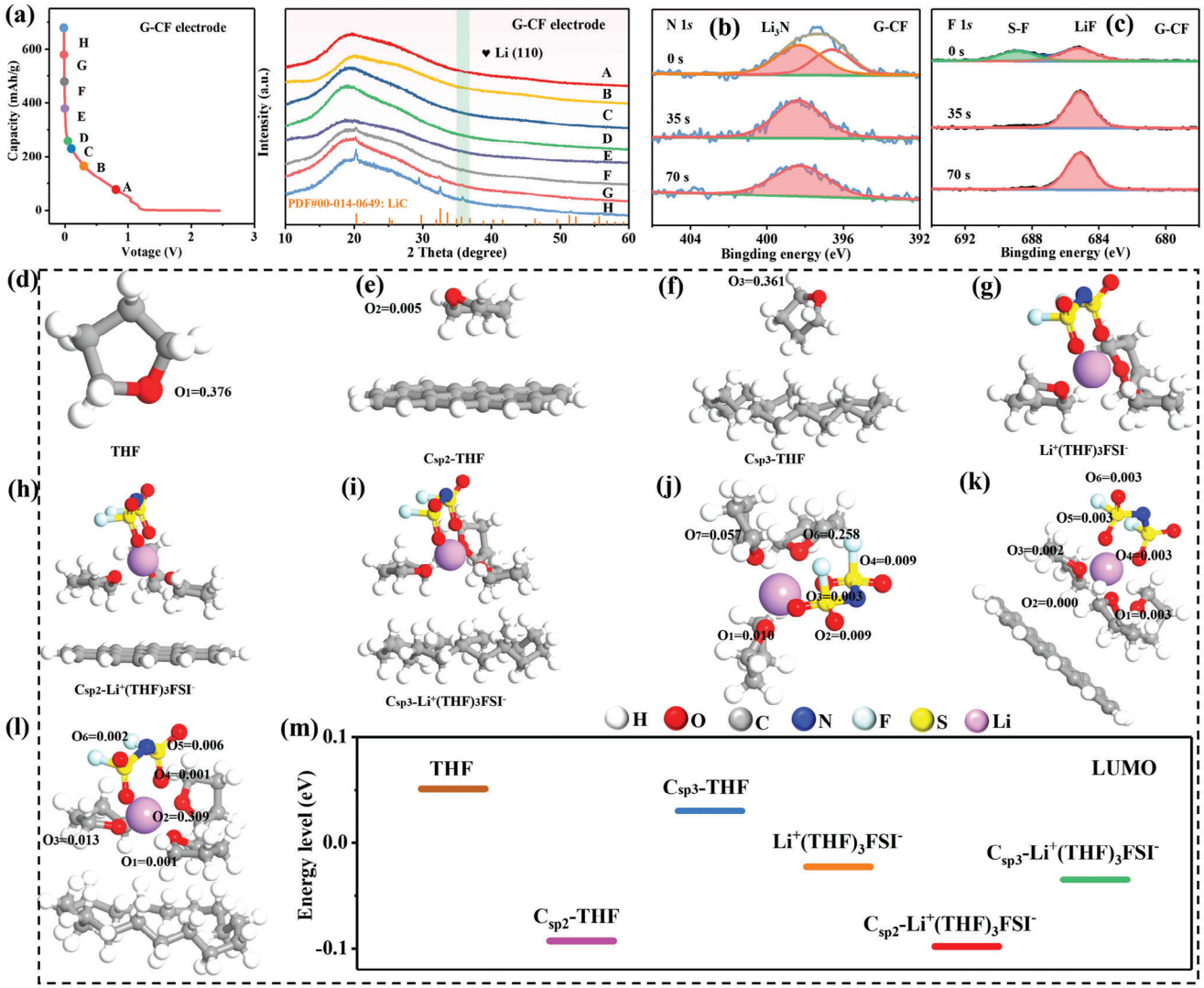

Figure 4. a) The ex situ XRD pattern of the G-CF||Li cell at various discharge stages. High-resolution b) N 1s spectra, and c) F 1s spectra of the G-CF electrode at different etching times. The optimized structures and electrophilic attack reactivity of O atoms in d) THF, e) C_{sp2}-THF, f) C_{sp3}-THF. The optimized structures g) $Li^+(THF)_3FSI^-$, h) C_{sp2}-$Li^+(THF)_3FSI^-$, and i) C_{sp3}-$Li^+(THF)_3FSI^-$ complexes. The electrophilic attack reactivity of O atoms in j) $Li^+(THF)_3FSI^-$, k) C_{sp2}-$Li^+(THF)_3FSI^-$, and l) C_{sp3}-$Li^+(THF)_3FSI^-$. m) The LUMO energies of the complexes.

forms of adsorption and co-intercalation.[19,42,43] The characteristic peak of G-CF at 22° seamlessly merges with the diffraction pattern of the substrate (polyimide film) used for testing (Figure S11, Supporting Information). When Li deposition begins (below 0 V), plated Li forms the LiC compound (PDF#00-014-0649) on the surface of the G-CF electrode. As Li further deposits, the Li metal phase, identified by the peak at ≈36°, gradually grows on the G-CF electrode. In contrast, no LiC compound is observed in the CF electrode after Li plating (Figure S12, Supporting Information). Electrochemical performance evaluations and ex situ XRD results jointly indicate that the presence of the LiC compound in G-CF significantly enhances its reversibility in hybrid Li-ion/metal storage, highlighting its crucial role in promoting efficient energy storage capabilities.

The thickness and composition of SEI layer on the electrode surface also affect the hybrid Li-ion/metal storage behavior. Firstly, HRTEM was utilized to analyze the thickness of SEI layer on the electrodes after 5 cycles. Figure S13a (Supporting Information) clearly demonstrates that the G-CF electrode exhibits notably thinner SEI layers, approximately 9.5 nm on the nanofiber, a markedly thinner layer than that formed on the CF electrode (Figure S13b, Supporting Information). XPS depth sputtering was conducted to reveal the SEI layer component of CF and G-CF electrodes after 5 cycles. It was found that the SEI layers of both electrodes contain C, N, O, S, F, and Li elements (Figure S14 and Table S3, Supporting Information). Notably, the C/O ratio can directly indicate different SEI components related to the electrodes.[24] After sputtering for 0, 35, and 70 s, the G-CF electrode consistently exhibits a higher C/O atomic ratio (2.0, 1.4, and 1.4, respectively) compared to the CF electrode (Figure S15, Supporting Information), indicating a lower degree of electrolyte reduction and thus a lower content of O-rich compounds. The

atomic ratios of N and F in the SEI layer of the G-CF electrode are 3.2% and 5.0% (Table S3, Supporting Information), respectively. From different etching times of N 1*s*, the main component is Li_3N, which is uniformly distributed in the SEI layer of G-CF and CF electrodes (Figures 4b and S16a, Supporting Information).[44] For F 1*s*, the main surface components of the electrode are LiF and S-F (Figures 4c and S16b, Supporting Information).[45,46] As etching proceeds, LiF is uniformly distributed in the inner layer of the SEI. This uniform distribution of Li_3N and LiF endows the SEI layer with excellent ion conductivity and mechanical properties, effectively reducing the formation of Li dendrites.[19,47] It is worth mentioning that the SEI layer rich in inorganic species can reduce the resistance for Li ions transport, thereby improving interfacial kinetics. From EIS results, the G-CF||Li cell exhibits faster kinetic in the range from room temperature to −20 °C (Figure S17, Supporting Information). In addition, from galvanostatic intermittent titration technique (GITT) results (Figure S18, Supporting Information), the Li^+ diffusion coefficient in the G-CF electrode is higher than that in the CF, further verifying the rapid Li storage kinetics achieved in the G-CF.[24] Therefore, the G-CF electrode shows ultra-high low-potential capacity and highly reversible hybrid Li ion/metal storage behavior.

To gain a deeper understanding of the formation of the SEI layer in the 1 M LiFSI-THF electrolyte, the lowest unoccupied molecular orbital (LUMO) energies and the electrophilic attack reactivity of O atoms were calculated to elucidate the role of C_{sp2} carbon structure in this process. As shown in Figure 4d–i, the free THF solvent molecule and the solvation sheath of $Li^+(THF)_3FSI^-$ are combined with C_{sp2} and C_{sp3} carbon species.[19] The LUMO energies of the THF molecule, C_{sp2}-THF, C_{sp3}-THF, $Li^+(THF)_3FSI^-$, C_{sp2}-$Li^+(THF)_3FSI^-$, and C_{sp3}-$Li^+(THF)_3FSI^-$ are 0.051, −0.093, 0.030, −0.023, −0.098, and −0.035 eV (Figure 4m), respectively. Additionally, In Figure 4d–f,j–l, the O atoms in THF (0.376 eV), C_{sp3}-THF (0.361 eV), $Li^+(THF)_3FSI$, and C_{sp3}-$Li^+(THF)_3FSI^-$ exhibit higher electrophilic attack reactivity than C_{sp2}-THF (0.005 eV) and C_{sp2}-$Li^+(THF)_3FSI^-$. This implies that the THF molecules are more easily reduced in the C_{sp3}-THF and C_{sp3}-$Li^+(THF)_3FSI^-$. Given that the G-CF surface is mainly composed of the C_{sp2} carbon structure, the dominant formation of the precursor C_{sp2}-THF and C_{sp2}-$Li^+(THF)_3FSI^-$ occurs before SEI layer formation. According to the analysis of LUMO and electrophilic attack reactivity, C_{sp2} is more electrophilic, resulting in the O atom of THF being less aggressive. This indicates that the C_{sp2} structure can effectively inhibit the decomposition of THF. This finding aligns with the CV results, which show that the intensity of the reduction peaks for G-CF||Li is lower than that for CF||Li at both 0.7 and 0.2 V (Figure S8, Supporting Information). This suggests that the graphitized layers with a high C_{sp2} structure effectively suppress the reduction of the electrolyte. Therefore, the presence of a high proportion C_{sp2} structure can achieve a higher ICE in the G-CF than in the CF electrode.

2.4. Electrochemical Performance of Full Cell

The G-CF electrode exhibits high ICE, stable capacity, and long-term cycling performance in half cells. This inspires us to evaluate the practical application in Li-free anode for hybrid LIB/LMBs full cells. As shown in **Figures** 5a and S19 (Supporting Information), the G-CF anode is directly matched with the NCM811 (or LFP) cathode with an N/P ratio of 0.5. This ensures that the Li provided by the NCM811 or LFP cathode can achieve a hybrid Li-ion/metal storage on the G-CF anode. Since the N/P ratio is 0.5, we calculate the capacity of the full cell based on the anode side. The average ICEs of the CF||NCM811 and G-CF||NCM811full cells are obtained by repeating 5 full cells. The G-CF||NCM811 full cells show an average ICE of 84.5% at 0.5 C (Figure 5b), which is higher than that of the CF||NCM811 full cells (74.4%). The increased ICE significantly reduces the irreversible capacity loss in the NCM811 cathode, thereby achieving higher reversible capacity and energy density in hybrid batteries. The full cell shows excellent rate performance, providing capacities of 584.8, 537.3, and 518.7 mA h g^{-1} at 0.5, 1, and 2 C, respectively (Figure 5c). The cycling performance of the G-CF||NCM811 full cell at 1 C is shown in Figure 5d. After three formation cycles, the G-CF||NCM811 full cell delivers a capacity of 530.8 mA h g^{-1} and a high energy density of 365.9 W h kg^{-1} (based on the active materials of anode and cathode, the energy densities mentioned later are all calculated based on this method). It remains stable over 50 cycles with a capacity retention rate of 93.2%. The charge–discharge profiles (Figure 5e) indicate that most of the capacity is concentrated in the range of 3.6–4 V, which is attributed to the synergistic effect of co-intercalation and Li plating on the G-CF anode. Even at 2 C, the G-CF||NCM811 full cell also provides a high voltage plateau and offers a capacity of 519.7 mA h g^{-1} and an energy density of 332.5 W h kg^{-1} (Figure 5f,g), remaining stable over 50 cycles. At the same N/P ratio, the G-CF||LFP full cell also provides a high voltage plateau (3.0–3.5 V) and a capacity of 541.0 mA h g^{-1} and remains stable over 100 cycles at 1 C (Figure 5h,i). In addition, the 30 mA h-level G-CF||NCM811 pouch cell can be stably cycled more than 100 times (Figure 5j), with a capacity retention of 83.1%, demonstrating good practical applications. Compared with the reported carbon materials for hybrid batteries, the G-CF||NCM811 full cell also demonstrates excellent ICE and cycling stability (Table S4, Supporting Information). In conclusion, encapsulating hard carbon with graphitized layers becomes a crucial strategy for developing advanced Li-free anodes for hybrid batteries, characterized by high ICE, long-term cycling stability, and high energy density.

3. Conclusion

In conclusion, we fabricated a heterogeneous structure where carbon nanofibers are encapsulated by graphitized layers and designed it as a Li-free anode for high-efficiency hybrid LIB/LMBs. The outer layer of this heterogeneous structure features a C_{sp2} carbon structure, which can effectively reduce side reactions with the electrolyte, promote the formation of LiC compound, and induce uniform Li plating/stripping, thereby enhancing the reversibility of hybrid Li ions/metal storage. Additionally, the amorphous carbon structure in the inner layer of the heterogeneous structure augments its fast-charging capability. As a result, the G-CF electrode achieves an optimal ICE of 85.2% and demonstrates long-term cycling performance. Under 2 C fast charging, the G-CF||Li cell maintains an average CE of 99.94% and a capacity of 500 mA h g^{-1} over 200 cycles. Moreover, when the N/P ratio is 0.5, the G-CF||NCM811 full cell exhibits an ICE of 84.5% and

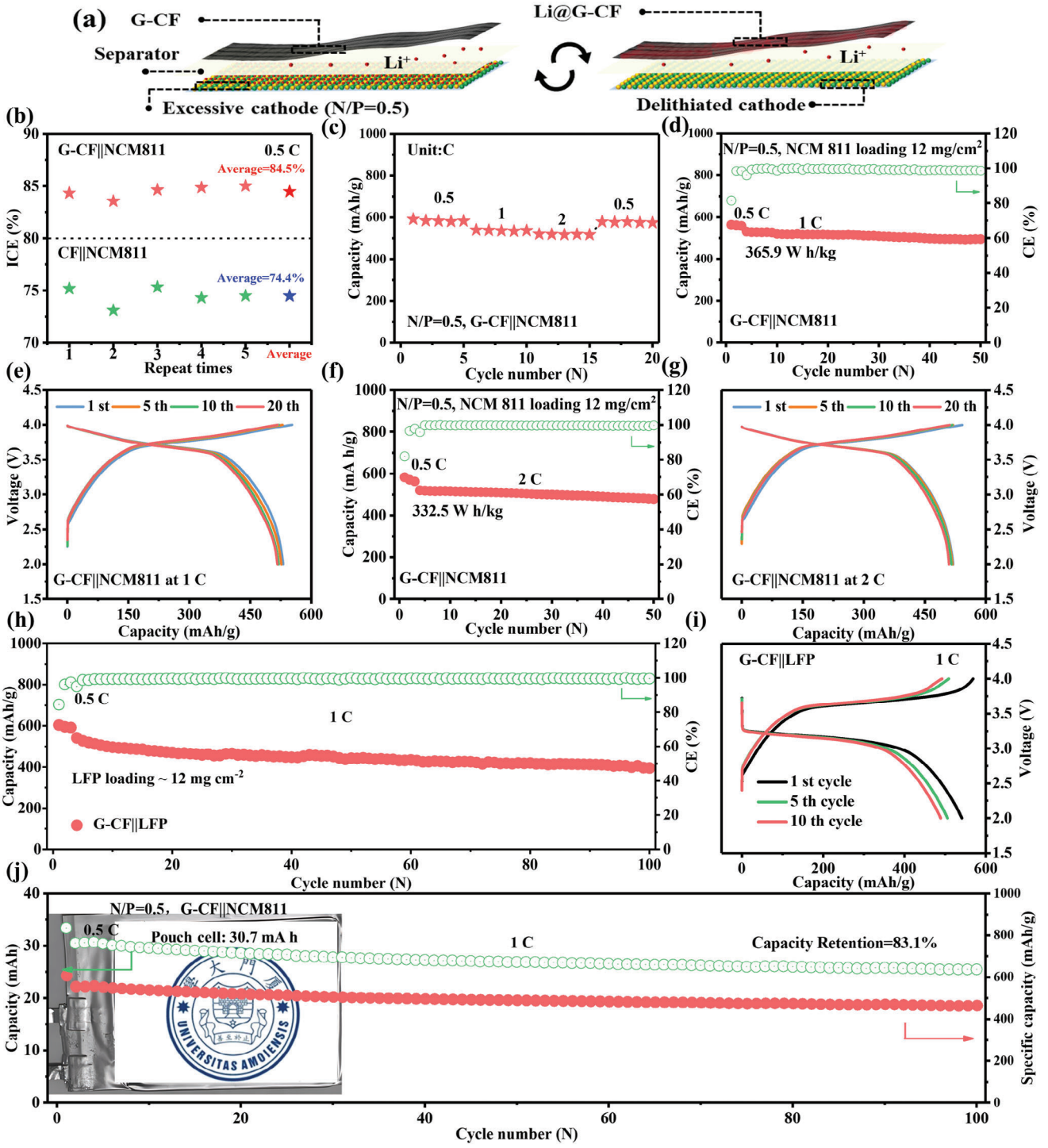

Figure 5. a) Schematic diagram of the G-CF||cathode with an N/P ratio of 0.5. b) The average ICEs are obtained by repeating tests on 5 full cells. c) Rate performance. d) The long-term cycling stability and e) corresponding charge–discharge profiles of the G-CF||NCM811 at 1 C. f) The long-term cycling stability and g) corresponding charge–discharge curves of the G-CF||NCM811 at 2 C fast charging. h) The long-term cycling stability and i) corresponding charge–discharge curves of the G-CF||LFP full cell at 1 C. j) The long-term cycling stability of the 30 mA h-level G-CF||NCM811 pouch cell at 1 C (the illustration is a digital photograph of the pouch cell).

provides a capacity of 530.8 mA h g^{-1} with an energy density of 365.9 W h kg^{-1}. The G-CF||LFP full cell can also offer a capacity of 541.0 mA h g^{-1} under the same N/P ratio. This work provides a significant reference for the design of advanced Li-free carbon anodes for hybrid LIB/LMBs with high ICE and long-term cycling stability.

Supporting Information

Supporting Information is available from the Wiley Online Library or from the author.

Acknowledgements

This work is supported by the National Natural Science Foundation of China (No. 31870570), the Science and Technology Plan of Fujian Provincial, China (No. 2020H4026, No. 2022H6002), and the Scientific Research Start-up Funding for Special Professor of Minjiang Scholars, Xiamen University.

Conflict of Interest

The authors declare no conflict of interest.

Data Availability Statement

The data that support the findings of this study are available from the corresponding author upon reasonable request.

Keywords

carbon nanofibers, graphitized layers, hybrid LIB/LMBs, joule heating, Li-free anodes

Received: December 20, 2024
Revised: January 15, 2025
Published online:

[1] J.-G. Zhang, W. Xu, J. Xiao, X. Cao, J. Liu, *Chem. Rev.* **2020**, *120*, 13312.
[2] J. Song, Y. Chen, H. Huang, J. Wang, S. C. Huang, Y. F. Liao, A. E. Fetohi, F. Hu, H. Chen, L. Li, X. Han, K. M. El-Khatib, S. Peng, *Adv. Sci.* **2022**, *9*, 2104522.
[3] C. Hu, G. Xing, W. Han, Y. Hao, C. Zhang, Y. Zhang, C. H. Kuo, H. Y. Chen, F. Hu, L. Li, S. Peng, *Adv. Mater.* **2024**, *36*, 2405763.
[4] A. Huang, Y. Ma, J. Peng, L. Li, S. Chou, S. Ramakrishna, S. Peng, *eScience* **2021**, *1*, 141.
[5] T. Lyu, F. Luo, D. Wang, L. Bu, L. Tao, Z. Zheng, *Adv. Energy Mater.* **2022**, *12*, 2201493.
[6] X. Yang, J. Liu, N. Pei, Z. Chen, R. Li, L. Fu, P. Zhang, J. Zhao, *Nano-Micro Lett.* **2023**, *15*, 75.
[7] J. Xiao, Q. Li, Y. Bi, M. Cai, B. Dunn, T. Glossmann, J. Liu, T. Osaka, R. Sugiura, B. Wu, J. Yang, J. G. Zhang, M. S. Whittingham, *Nat. Energy* **2020**, *5*, 561.
[8] Z. Piao, R. Gao, Y. Liu, G. Zhou, H. M. Cheng, *Adv. Mater.* **2023**, *35*, 2206009.
[9] L. Tao, B. Ma, F. Luo, Z. Xu, Z. Zheng, H. Huang, P. Bai, F. Lin, *Nano Energy* **2022**, *93*, 106808.
[10] R. Zhang, X. R. Chen, X. Chen, X. B. Cheng, X. Q. Zhang, C. Yan, Q. Zhang, *Angew. Chem., Int. Ed.* **2017**, *56*, 7764.
[11] T. Lyu, F. Luo, Z. Wang, F. Jiang, S. Geng, Y. Zhuang, X. Lin, J. Chen, D. Wang, L. Bu, L. Tao, L. Liang, Z. Zheng, *Chem. Eng. J.* **2023**, *466*, 143357.
[12] P. Xue, C. Sun, H. Li, J. Liang, C. Lai, *Adv. Sci.* **2019**, *6*, 1900943.
[13] F. Luo, D. Xu, Y. Liao, M. Chen, S. Li, D. Wang, Z. Zheng, *J. Energy Chem.* **2023**, *77*, 11.
[14] C. Martin, M. Genovese, A. J. Louli, R. Weber, J. R. Dahn, *Joule* **2020**, *4*, 1296.
[15] X. Yue, J. Zhang, Y. Dong, Y. Chen, Z. Shi, X. Xu, X. Li, Z. Liang, *Angew. Chem., Int. Ed.* **2023**, *62*, 202302285.
[16] T. Zhou, J. Shen, Z. Wang, J. Liu, R. Hu, L. Ouyang, Y. Feng, H. Liu, Y. Yu, M. Zhu, *Adv. Funct. Mater.* **2020**, *30*, 1909159.
[17] R. Wang, R. Wu, X. Yan, D. Liu, P. Guo, W. Li, H. Pan, *Adv. Funct. Mater.* **2022**, *32*, 2200424.
[18] Y. Dong, Y. Chen, X. Yue, Z. Liang, *Energy Environ. Sci.* **2024**, *17*, 2500.
[19] T. Lyu, F. Luo, L. Liang, D. Wang, L. Tao, Z. Zheng, *Adv. Energy Mater.* **2024**, *14*, 2304520.
[20] Y. Fang, S. L. Zhang, Z.-P. Wu, D. Luan, X. W. Lou, *Sci. Adv.* **2021**, *7*, eabg3626.
[21] Z. Xu, L. Xu, Z. Xu, Z. Deng, X. Wang, *Adv. Funct. Mater.* **2021**, *31*, 2102354.
[22] J. Xiao, N. Xiao, K. Li, L. Zhang, J. Chang, X. Ma, H. Li, J. Bai, Q. Jiang, J. Qiu, *Adv. Energy Mater.* **2022**, *12*, 2103123.
[23] L. Tao, A. Hu, Z. Yang, Z. Xu, C. E. Wall, A. R. Esker, Z. Zheng, F. Lin, *Adv. Funct. Mater.* **2020**, *30*, 2000585.
[24] L. Tao, P. Sittisomwong, B. Y. Ma, A. Y. Hu, D. W. Xia, S. Hwang, H. B. Huang, P. Bai, F. Lin, *Energy Storage Mater.* **2023**, *55*, 826.
[25] T. Lyu, X. Lan, L. Liang, X. Lin, C. Hao, Z. Pan, Z. Q. Tian, P. K. Shen, *Electrochim. Acta* **2021**, *365*, 137356.
[26] A. Huang, Y. Wu, H. Huang, C. Li, Y. Sun, L. Li, S. Peng, *Adv. Funct. Mater.* **2023**, *33*, 2303111.
[27] H. Huang, A. Huang, D. Liu, W. Han, C.-H. Kuo, H.-Y. Chen, L. Li, H. Pan, S. Peng, *Adv. Mater.* **2023**, *35*, 2303109.
[28] J. Kang, Y. Ko, J. P. Kim, J. Y. Kim, J. Kim, O. Kwon, K. C. Kim, D. W. Kim, *Nat. Commun.* **2023**, *14*, 901.
[29] S. Li, G. Xing, S. Zhao, J. Peng, L. Zhao, F. Hu, L. Li, J. Wang, S. Ramakrishna, S. Peng, *Nat. Sci. Rev.* **2024**, *11*, nwae193.
[30] W. Chen, M. Niu, Z. Zhang, L. Chen, X. Li, J. Zhang, R. Sun, H. Cao, X. Wang, *Small* **2024**, *20*, 2311026.
[31] X. Gao, Y. Sun, B. He, Y. Nuli, J. Wang, J. Yang, *ACS Energy Lett.* **2024**, *9*, 1141.
[32] L. Xie, C. Tang, Z. Bi, M. Song, Y. Fan, C. Yan, X. Li, F. Su, Q. Zhang, C. Chen, *Adv. Energy Mater.* **2021**, *11*, 2101650.
[33] M. Wang, Z. Ren, Z. Chen, H. Lin, J. Yan, Z. Lu, S. Chen, H. Li, Y. Shen, M. Xie, M. Wang, D. Wang, *Mater. Today Energy* **2022**, *29*, 101134.
[34] Z. Yu, D. Han, J. Chen, Z. Xu, X. Liu, S. Yang, Y. Liu, *Electrochim. Acta* **2022**, *422*, 140552.
[35] S. Xia, Q. Guo, Y. Yu, Y. Li, S. Wang, D. Dong, Z. Liu, H. Zhou, X. Zhou, Z. Liu, *Carbon* **2023**, *203*, 743.
[36] B. Sun, Q. Zhang, W. Xu, R. Zhao, H. Zhu, W. Lv, X. Li, N. Yang, *Nano Energy* **2022**, *94*, 106937.
[37] Y. Liu, C. Sun, Y. Lu, X. Lin, M. Chen, Y. Xie, C. Lai, W. Yan, *Chem. Eng. J.* **2023**, *451*, 138570.
[38] D. Xie, H.-H. Li, W.-Y. Diao, R. Jiang, F.-Y. Tao, H.-Z. Sun, X.-L. Wu, J.-P. Zhang, *Energy Storage Mater.* **2021**, *36*, 504.
[39] X. Liu, Q. Zhang, Y. Ma, Z. Chi, H. Yin, J. Liu, J. Huang, Z. Guo, L. Wang, *J. Energy Chem.* **2022**, *69*, 270.
[40] W. Liu, P. Zhai, S. Qin, J. Xiao, Y. Wei, W. Yang, S. Cui, Q. Chen, C. Jin, S. Yang, Y. Gong, *J. Energy Chem.* **2021**, *56*, 463.
[41] H. Gong, Y. Chen, S. Chen, C. Xu, Y. Yang, Y. Ye, Z. Huang, R. Ning, Y. Cui, Z. Bao, *ACS Energy Lett.* **2022**, *7*, 4417.

[42] S. Alvin, H. S. Cahyadi, J. Hwang, W. Chang, S. K. Kwak, J. Kim, *Adv. Energy Mater.* **2020**, *10*, 2000283.
[43] B. Liu, K. Jiang, K. Zhu, X. Liu, K. Ye, J. Yan, G. Wang, D. Cao, *Chem. Eng. J.* **2022**, *446*, 137208.
[44] X. Xu, X. Yue, Y. Chen, Z. Liang, *Angew. Chem., Int. Ed.* **2023**, *62*, 202306963.
[45] W. Xue, Z. Shi, M. Huang, S. Feng, C. Wang, F. Wang, J. Lopez, B. Qiao, G. Xu, W. Zhang, Y. Dong, R. Gao, Y. Shao-Horn, J. A. Johnson, J. Li, *Energy Environ. Sci.* **2020**, *13*, 212.
[46] T. D. Pham, A. B. Faheem, K. K. Lee, *Small* **2021**, *17*, 2103375.
[47] X. Shi, J. Liu, H. Zhang, Z. Xue, Z. Zhao, Y. Zhang, G. Wang, L. Akbar, L. Li, *ACS Nano* **2024**, *18*, 8827.